Journal of Materials Chemistry B

ROYAL SOCIETY OF CHEMISTRY

PAPER

View Article Online
View Journal | View Issue

Cite this: J. Mater. Chem. B, 2022, 10, 5594

Construction of a gold nanoparticle-based single-molecule biosensor for simple and sensitive detection of Argonaute 2 activity†

Su Jiang,‡[a] Xinyi Zhang,‡[b] Dong-ling Li,[a] Ting-ting Wang,[a] Fei Ma*[c] and Chun-Yang Zhang *[a]

Received 12th April 2022,
Accepted 28th June 2022

DOI: 10.1039/d2tb00802e

rsc.li/materials-b

Argonaute 2 (Ago2) is an essential component of the RNA-induced silencing complex (RISC) and it participates in diverse physiological processes, while dysregulation of Ago2 activity is closely linked to a variety of human diseases including cancers. The reported Ago2 assays often suffer from laborious procedures, complicated reaction schemes, and unsatisfactory sensitivity. Herein, we develop a new gold nanoparticle (AuNP)-based single-molecule biosensor for simple and sensitive detection of Ago2 activity. The Ago2-responsive AuNP nanoprobe is constructed through the self-assembly of multiple Cy5-labeled signal probes onto the AuNP, in which the Cy5 fluorescence is efficiently quenched by the AuNP. Target Ago2 can bind with guide RNA to form an active RISC, inducing the cyclic cleavage of the signal probes and the release of Cy5 moieties from the AuNP nanoprobe. The released Cy5 molecules can be simply quantified by single-molecule counting. This single-molecule biosensor enables detection of Ago2 activity with the involvement of only a single AuNP nanoprobe, eliminating the use of any extra antibodies and protein enzymes. This single-molecule biosensor achieves good specificity and high sensitivity with a detection limit of 9.1 pM, and it can be exploited for the screening of Ago2 inhibitors, Ago2 kinetic analysis, and the imaging of intracellular Ago2 activity in live cells, holding great promise in Ago2-related biomedical research and clinical diagnosis.

1. Introduction

Argonaute 2 (Ago2) is an indispensable component of the RNA-induced silencing complex (RISC) which is involved in RNA interference-mediated gene regulation processes.[1–3] Upon binding to single-stranded guide RNA (*e.g.*, miRNA, siRNA, and piRNA), Ago2 can recognize the target mRNA through specific Watson–Crick base-pairing between guide RNA and mRNA, and subsequently catalyze the cleavage of the mRNA strand to induce translation inhibition/repression.[4–6] Ago2 extensively participates in a series of cellular physiological processes including proliferation, differentiation, and apoptosis,[7–10] while abnormal expression of Ago2 will disturb the gene regulation system and consequently leads to diverse human diseases including breast cancer,[11] ovarian cancer,[12,13] gastric cancer,[14] and lung cancer.[15,16] Therefore, the development of efficient biosensors for the Ago2 assay will greatly facilitate RNA interference-related biomedical research and clinical diagnosis.

Western blotting[17] and enzyme-linked immunosorbent assay[18] are most widely used for Ago2 detection. However, they involve tedious procedures with poor specificity due to the use of unstable antibodies for target recognition, and they can only detect the content of Ago2 protein instead of its activity. Alternatively, a G-quadruplex–hemin complex-based electrochemical biosensor is constructed to detect the cleavage activity of Ago2 with high selectivity and excellent reproducibility,[19] but it still requires complicated steps for the preparation of the working electrode. Fluorescent biosensors based on molecular beacons,[20] DNA tetrahedra,[21] and graphene oxide[22] enable the detection of Ago2 activity in a homogenous manner, but they suffer from a relatively high background signal as a result of incomplete fluorescence quenching and poor sensitivity due to the lack of signal amplification. To improve the sensitivity, rolling-circle amplification is further introduced to efficiently amplify the Ago2 signal,[23,24] but additional enzymes (*e.g.*, phi29 DNA polymerase and Bst DNA polymerase) and DNA strands (*e.g.*, circular template, dual-labeled signal probe, and second

[a] College of Chemistry, Chemical Engineering and Materials Science, Shandong Normal University, Jinan 250014, China. E-mail: cyzhang@sdnu.edu.cn
[b] School of Chemistry and Chemical Engineering, Guangdong Pharmaceutical University, Zhongshan 528458, China
[c] School of Chemistry and Chemical Engineering, Southeast University, Nanjing 211189, China. E-mail: fei@seu.edu.cn

† Electronic supplementary information (ESI) available. See DOI: https://doi.org/10.1039/d2tb00802e

‡ These authors contributed equally.

primer) are required to implement the amplification reaction, which inevitably increases the assay cost and complexity.

Gold nanoparticles (AuNPs) are one of the most popular nanomaterials for biosensing applications due to their unique optical and electrical properties, large surface area, easy surface modification, excellent biocompatibility, high extinction coefficients, and potential noncytotoxicity.[25–28] Herein, we develop a new gold nanoparticle-based single-molecule biosensor for simple and sensitive detection of Ago2 activity. In this biosensor, multiple Cy5-labeled signal probes are assembled on AuNPs to construct a fluorescence-quenched AuNP nanoprobe. Target Ago2 catalyzes the cyclic cleavage of signal probes upon the binding of active RISC with guide RNA, releasing large amounts of Cy5 moieties from the AuNP nanoprobe. The released Cy5 molecules can be quantified *via* single-molecule counting. This single-molecule biosensor is very simple with the requirement of only a single AuNP nanoprobe, and it can further be applied for the screening of Ago2 inhibitors and the measurement of endogenous Ago2 activity in different kinds of human cells.

2. Experimental

2.1 Chemicals and materials

All oligonucleotides were synthesized by Takara Biotechnology Co. Ltd (Dalian, China). The sequences are listed in Table 1. Recombinant mammalian Ago2 was purchased from Sino Biological Inc. (Beijing, China). DEPC-treated water was obtained from Shanghai Sangon Biological Engineering Technology & Services Co. Ltd (Shanghai, China). The RNase inhibitor was obtained from Takara Biotechnology Co. Ltd (Dalian, China). (±) – 6-Hydroxy-2,5,7,8-tetramethylchromane-2-carboxylic acid (trolox), trizma hydrochloride (Tris–HCl), sodium chloride (NaCl), di-sodium hydrogen phosphate (Na_2HPO_4), sodium dihydrogen phosphate (NaH_2PO_4), ethylenediaminetetraacetic acid (EDTA) potassium chloride (KCl), magnesium chloride ($MgCl_2$), endoproteinase rLys-C, bovine serum albumin (BSA), and α-thrombin from human plasma were obtained from Sigma-Aldrich Company (St. Louis, MO, USA). The p19 siRNA binding protein was purchased from New England Biolabs (Beverly, MA, USA). Dithiothreitol (DTT) was obtained from Invitrogen (Carlsbad, CA). The human lung adenocarcinoma cell line (A549 cells), human cervical carcinoma cell line (HeLa cells), human colon carcinoma cell line (HCT116 cells), and human breast cancer cell line (MCF-7 cells) were purchased from Cell Bank, Shanghai Institutes for Biological Sciences, Chinese Academy of Sciences (Shanghai, China). 10 nm Au nanoparticles were bought from Nanocs, Inc. (New York, USA). Aurintricarboxylic acid (ATA), suramin sodium salt (SA) and oxidopamine HCl (6-OHDA HCl) were bought from Macklin (Shanghai, China). The Lipofectamine 3000 transfection reagent, Opti-MEM I reduced-serum medium, McCoy's 5A (modified) medium, Dulbecco's modified Eagle's medium (DMEM) and 10% fetal bovine serum (FBS) were bought from Thermo Fisher Scientific (Massachusetts, USA). 1% Penicillin-streptomycin was purchased from Invitrogen Corporation (Carlsbad, CA, USA). All solutions were prepared using DEPC-treated water. Other chemical reagents were analytical grade and used without further purification.

Table 1 Sequences of the oligonucleotides[a]

Oligonucleotide	Sequence (5′ → 3′)
Guide RNA	PO_4-UGG AGU GUG ACA AUG GUG UUU G
Signal probe	SH-CAA ACA CCA UUG UCA CAC UCC A-Cy5

2.2 Preparation of the AuNP nanoprobe

The AuNPs (10 nm) were modified with signal probes using the salt aging method. 10 μL of 100 μM signal probe and AuNP solution (1 mL, 5.7×10^{12} particles per mL) were mixed at room temperature for 4 min, followed by standing for 20 min. Then 1 × PBS buffer (10 mM phosphate (NaH_2PO_4/Na_2HPO_4) and 1% tween 20, pH 7.4) was added into the solution and mixed at room temperature for 4 min, followed by standing for 20 min. Then the NaCl concentration was increased to 0.3 M over 24 h in a stepwise manner and incubated at 4 °C for another 24 h. To remove the excess signal probes, the suspension was centrifuged at 20 000 rcf for 30 min, and the supernatants were removed. The resultant AuNP nanoprobes were resuspended in PBS buffer (10 mM phosphate and 0.1 M NaCl, pH 7.0) and stored at 4 °C for further use.

2.3 Detection of Ago2 activity

A 10 μL solution containing target Ago2 with different concentrations, 100 nM guide RNA, and 1× Ago2 reaction buffer (30 mM Tris buffer, pH 7.5, 130 mM KCl, 1.1 mM $MgCl_2$, 1 mM DTT, and 0.1 mM EDTA) was incubated at 30 °C for 30 min to form the RISC. Then 0.5 μL of the AuNP nanoprobe and 0.5 μL of 10× Ago2 reaction buffer (300 mM Tris buffer, pH 7.5, 1.3 M KCl, 11 mM $MgCl_2$, 10 mM DTT, and 1 mM EDTA) were added to the solution with a total volume of 15 μL, followed by incubation at 30 °C for 60 min. The reaction products were diluted to 50 μL using DEPC-treated water and centrifuged at 20 000*g* for 20 min, and the supernatant was subjected to further measurements.

2.4 Gel electrophoresis analysis

15 μL of the cleavage reaction products were analyzed by 15% nondenaturing polyacrylamide gel electrophoresis (PAGE) on ice at a 130 V constant voltage for 50 min in 1× TBE buffer (9 mM Tris–HCl, pH 7.9, 9 mM boric acid, and 0.2 mM EDTA). The gels were imaged using a Bio-Rad ChemiDoc MP imaging system (California, USA).

2.5 Steady-state fluorescence measurements

The fluorescence emission spectra were measured using an FLS-1000 fluorescence spectrophotometer (Edinburgh, UK). An excitation wavelength of 635 nm was used to measure the fluorescence intensity, and the spectra were recorded from 650 to 800 nm. The excitation and emission bandwidths were set at 6 nm.

2.6 Single-molecule detection

For total internal reflection fluorescence (TIRF) imaging, an Olympus IX-71 inverted microscope (Olympus, Tokyo, Japan) equipped with a UAPON 100× TIRF objective (1.49 NA,

Olympus) was used. A 640 nm laser was used to excite Cy5. For each sample, 50 μL of the final product was diluted 100 times. Then 10 μL of the diluted solution was measured and imaged with an exposure time of 100 ms. All the images were quantitatively analyzed using ImageJ software (version 1.48e19, Broken Symmetry Software, USA). The size of the particles was set at ≥2 pixels to reduce false positive signals resulting from noise. For data analysis, a region of interest (ROI) with 600 × 600 pixels was selected for single-molecule counting. For each sample, the fluorescent spots were analyzed in 10 frames, and the number of fluorescent molecules counted (N) is the average number in 10 frames.

2.7 Inhibition assay

For the Ago2 inhibition assay, 9 μL of the reaction mixture containing the inhibitor with indicated concentrations, 0.67 μL of 1.5 μM Ago2, and 1 μL of 10× reaction buffer (300 mM Tris buffer, pH 7.5, 1.3 M KCl, 11 mM $MgCl_2$, 10 mM DTT, and 1 mM EDTA) was incubated at 30 °C for 20 min. Subsequently, 1 μL of 1 μM guide RNA was added into the mixture and incubated at 30 °C for 30 min. The Ago2 activity assay was performed following the same procedures described above.

2.8 Preparation of cell extracts

The human cervical carcinoma cell line (HeLa cells), human lung adenocarcinoma cell line (A549 cells), and human breast adenocarcinoma cell line (MCF-7 cells) were cultured in Dulbecco's modified Eagle's medium (DMEM) containing 1% penicillin-streptomycin and 10% FBS in a humidified chamber containing 5% CO_2 at 37 °C. The human colon carcinoma cell line (HCT116 cells) was cultured in McCoy's 5A (modified) medium containing 1% penicillin-streptomycin and 10% FBS. The whole-cell extracts were prepared according to the manufacturer's instructions, and the buffer solutions were obtained from the Nuclear Extract kit (Active Motif, Carlsbad, CA). Briefly, the cells were washed twice with 8 mL of ice-cold PBS/phosphatase inhibitor buffer, gently scrapped with a cell lifter and transferred to a pre-chilled 2 mL tube. The cell suspension was centrifuged for 5 min at 200 g at 4 °C, with the supernatant being discarded. The cell pellet was resuspended in 300 μL of the lysis buffer and placed on ice for 3 min by pipetting up and down at a 2 min interval. The suspension was vortexed for 30 sec and centrifuged at 4 °C for 20 min at 14 000g. The supernatant was transferred into a pre-cooled microcentrifuge tube and stored at −80 °C. The supernatant equivalent to 1×10^6 cells was used for the Ago2 activity assay.

2.9 Live cell imaging

About 2×10^6 HeLa cells grown on 20 mm Petri dishes were incubated for 12 h in a humidified incubator containing 5% CO_2 at 37 °C and used for live cell imaging. The Opti-MEM transfection mixture was prepared according to the manufacturer's instructions. Firstly, solution 1 (250 μL of Opti-MEM and 7.5 μL of Lipofectamine 3000) was mixed with solution 2 (250 μL of Opti-MEM, 10 μL of P3000TM, 10 μL of 10 μM guide RNA, and 10 μL of 0.19 μM nanoprobe) for 15 min at room temperature. Secondly, HeLa cells were gently washed twice with 1× PBS buffer (pH 7.4) and then incubated with the Opti-MEM transfection mixture for 2 h in a humidified incubator containing 5% CO_2 at 37 °C. Thirdly, after the transfection, the cells were gently washed ten times with 1× PBS buffer (pH 7.4) and 1 mL of DMEM solution containing 1% penicillin-streptomycin and 10% FBS was added into Petri dishes. The cell fluorescence images were obtained by using an Olympus IX-71 inverted microscope (Olympus, Japan) with a 10× objective. For the inhibition assay, the HeLa cells were pre-incubated in 500 μL of Opti-MEM medium containing 20 μL of 50 mM ATA inhibitor for 30 min. The live cell imaging was performed following the same procedures described above.

3. Results and discussion

3.1 Principle of the Ago2 assay

As shown in Scheme 1, a 22 nt single-stranded RNA is designed as a signal probe, which is labelled with a sulfhydryl group (SH) at the 5′ end and a Cy5 fluorophore at the 3′ end. Multiple signal probes can be assembled on the AuNP surface *via* Au–S bonding to obtain a AuNP nanoprobe, leading to efficient quenching of Cy5 fluorescence by AuNPs through static quenching and fluorescence resonance energy transfer[29,30] and consequently the generation of a low background when Ago2 is absent. The guide RNA (gRNA) sequence is identical to that of miR-122, and it is fully complementary to the signal probe. The gRNA possesses a 5′ phosphate (PO_4) end that can increase the Ago2 activity through stabilizing the RISC structure (see Fig. S1, ESI†).[31] Once target Ago2 binds with the signal

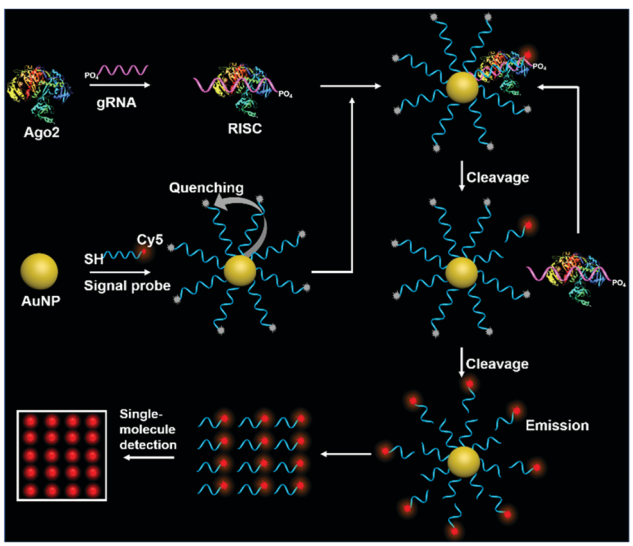

Scheme 1 Schematic illustration of the AuNP-based single-molecule biosensor for simple and sensitive detection of Ago2 activity.

probe, an activated RISC is formed and it subsequently cleaves the signal probe to releases the Cy5 moiety from the AuNP nanoprobe. Notably, the RISC disassociated from the cleaved signal probe can recognize a new signal probe to trigger the next round of cleavage reaction. As a result, multiple signal probes can be cyclically digested, releasing abundant Cy5 moieties from the AuNP nanoprobe. The released Cy5 molecules can be quantified by single-molecule counting. Notably, the AuNP nanoprobe is constructed through self-assembly of multiple signal probes on a single AuNP, which greatly improves the Ago2 cleavage efficiency through increasing the local concentration of substrate signal probes.[29,30] Moreover, only a AuNP nanoprobe is required for Ago2 sensing, without the requirement of any antibodies for target recognition and enzymes for signal amplification.

3.2 Feasibility of the Ago2 assay

Transmission electron microscopy (TEM) imaging demonstrates the similar morphology of bare AuNPs (Fig. 1A) and AuNP nanoprobes (Fig. 1B) with a diameter of 10 nm. Moreover, the signal probe exhibits characteristic absorption peaks of RNA at 260 nm and Cy5 at 650 nm (Fig. 1C, black line), and the bare AuNP has a characteristic absorption peak at 525 nm (Fig. 1C, red line). As expected, the AuNP nanoprobe exhibits all three characteristic absorption peaks (260 nm, 525 nm, and 650 nm, Fig. 1C, blue line), indicating the successful assembly of signal probes on the AuNP surface. The 15% polyacrylamide gel electrophoresis (PAGE) analysis (Fig. 1D) shows no distinct band in the control group without Ago, while a clear Cy5 band is observed upon Ago treatment. This result is consistent with that obtained by ensemble fluorescence measurements with the generation of an enhanced Cy5 signal upon Ago2 treatment (Fig. 1E, red line), but no obvious signal in the control group without Ago2 (Fig. 1E, black line). These results clearly demonstrate the successful fabrication of an Ago2-responsive AuNP-based fluorescent nanoprobe.

3.3 Sensitivity detection of Ago2 activity

Single-molecule detection can accurately quantify the target molecules by simply counting the individual fluorescent bursts, with distinct advantages of an ultrahigh sensitivity, a high signal-to-noise ratio, and low sample consumption.[32,33] When the target is absent, no fluorescent spot is observed (Fig. 2A), while abundant Cy5 spots are generated in response to target Ago2 (Fig. 2B). Under the optimal reaction conditions (see Fig. S2, ESI†), we investigated the sensitivity of the proposed single-molecule biosensor (Fig. 2C). The Cy5 count increases gradually with increasing concentration of Ago2 from 0 to 200 nM. In logarithmic scales, the Cy5 count (N) exhibits a linear correlation with the Ago2 concentration (C) in the range from 0.02 to 50 nM, with the correlation equation being $N = 92.79 \log_{10} C + 206.22$ ($R^2 = 0.9942$). The limit of detection is calculated to be 9.12×10^{-12} M (9.12 pM) based on the $3\sigma/K$ method, where σ is the standard deviation of the control group and K is the slope of the linear regression curve. Notably, the sensitivity of the proposed single-molecule biosensor is superior to the reported Ago2 assays (Table 2), which is 65.93-fold higher than that of a molecular beacon-based fluorescence assay (0.6 nM),[20] 186.81-fold higher than that of a graphene oxide-based fluorescence assay (1.7 nM),[22] 498.90-fold higher than that of a DNA tetrahedron-based fluorescent biosensor (4.54 nM),[21] and 551.65-fold higher than that of a G-quadruplex–hemin complex-based electrochemical biosensor (5.02 nM).[19] The high sensitivity of the proposed biosensor can be attributed to (1) the low background resulting from efficient quenching of the signal probes by AuNPs,[29] (2) efficient Ago2 signal amplification induced by the assembly of multiple signal probes on a single AuNP which greatly increases the local effective concentration of

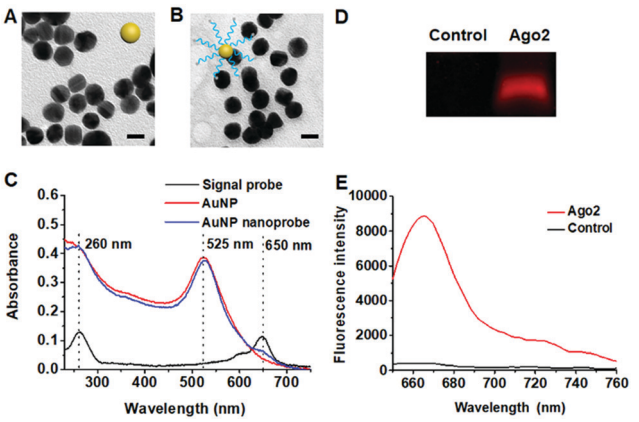

Fig. 1 (A) TEM images of bare AuNPs. (B) TEM images of AuNP nanoprobes. The scale bar is 10 nm. (C) UV-Vis absorption spectra of the signal probe (5 μM, black color), bare AuNP (red color), and AuNP nanoprobe (blue color). (D) PAGE analysis of the cleavage reaction products in the absence (control) and presence of 100 nM Ago2. The gel is imaged by direct excitation of Cy5. (E) Measurement of the Cy5 fluorescence signal in the absence (control, black line) and presence of 100 nM Ago2 (red line).

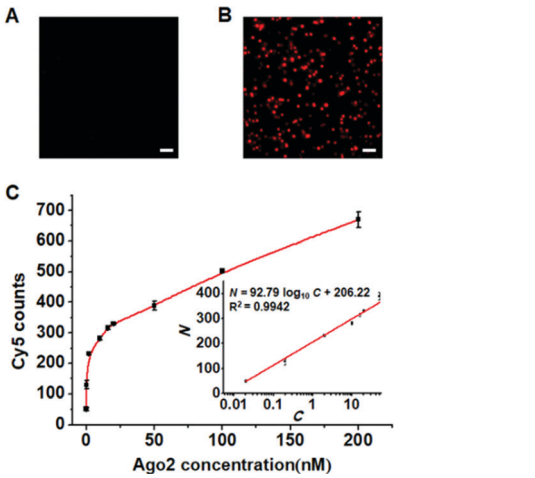

Fig. 2 (A) Single-molecule imaging of Cy5 moieties in the absence of Ago2. (B) Single-molecule imaging of Cy5 moieties in the presence of Ago2. The scale bar is 2 μm. (C) Variation of Cy5 count with the Ago2 concentration. Linear relationship between the Cy5 count and the logarithm of the Ago2 concentration (inset) in the range from 0.02 to 50 nM. Error bars show the standard deviation of three experiments.

Table 2 Comparison of the proposed biosensor with the reported methods for the Ago2 assay

Strategy	Kinetic analysis	Linear range	LOD	Assay time	Ref.
Branched rolling circle amplification-based fluorescence assay	ND	ND	10 nM	3.5 h	23
G-quadruplex-based electrochemical assay	ND	6.25–25 nM	5.02 nM	1.5 h	36
DNA tetrahedron-based fluorescence assay	ND	0–100 nM	4.54 nM	>4 h	37
Graphene oxide-based fluorescence assay	ND	5–35 nM	1.7 nM	1.5 h	22
Molecular beacon-based fluorescence assay	ND	1–25 nM	0.6 nM	>0.5 h	20
Gold nanoparticle-based single-molecule fluorescence assay	Yes	0.02–20 nM	9.1 pM	1.5 h	This work

the signal probes and accelerates the Ago2 cleavage reaction,[29,30] and (3) the inherent ultrahigh sensitivity of single-molecule counting.[32]

3.4 Selectivity of Ago2 assay

We further investigated the specificity of the proposed biosensor using the p19 siRNA binding protein (p19), thrombin, bovine serum albumin (BSA), rLys-C endoproteinase (rLys-C), Ago1, and Ago3 as the interferences (Fig. 4). p19 is an RNA silencing suppressor that can specifically bind siRNA with high affinity (K_d = 0.17 nM).[34,35] BSA is frequently used as an irrelevant protein.[38] Thrombin is a coagulation factor and a serine endopeptidase, and it can hydrolyze the peptide and ester bonds specifically at the carboxylic side of Arg.[39] rLys-C endoproteinase can specifically recognize and cleave the C-terminal peptide bonds in the peptide chain.[40] In theory, none of the above substances possesses cleavage activity toward the signal probe, and thus no Cy5 signal can be generated. As expected, a highly fluorescent signal is obtained only in response to target Ago2 (Fig. 3, red column), but no obvious signal is detected in response to p19 (Fig. 3, green column), thrombin (Fig. 3, blue column), BSA (Fig. 3, yellow column), rLys-C endoproteinase (Fig. 3, magenta column), Ago1 (Fig. 3, orange column), Ago3 (Fig. 3, purple column), and the control group without any protein/enzyme (Fig. 3, black column). These results demonstrate that the proposed biosensor processes excellent specificity toward Ago2. Moreover, the proposed biosensor exhibits good reproducibility (see Fig. S3, ESI†).

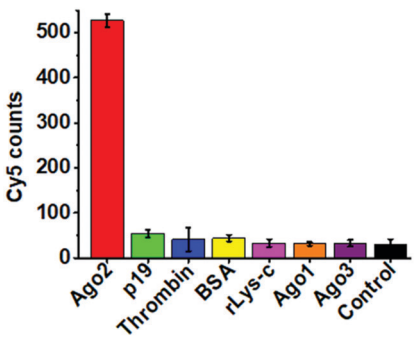

Fig. 3 Measurement of Cy5 count in response to Ago2 (100 nM, red column), p19 (100 U mL^{-1}, green column), thrombin (100 nM, blue column), BSA (100 nM, yellow column), rLys-C (100 nM, pink column), Ago1 (100 nM, orange column), Ago3 (100 nM, purple column), and the control group without any proteins/enzymes (black column). Error bars represent the standard derivation from three independent measurements.

3.5 Inhibition and kinetic analysis

We investigated the feasibility of the proposed biosensor for the inhibition assay using three small molecules including aurintricarboxylic acid (ATA), suramin (SA), and 6-hydroxydopamine hydrochloride (6-OHDA HCL) as the inhibitors. These inhibitors can decrease the Ago2 cleavage activity through hindering the binding of Ago2 with gRNA.[41] The relative activity of Ago2 decreases with increasing concentrations of ATA (Fig. 4A), SA (Fig. 4B), and 6-OHDA HCL (Fig. 4C), respectively. The relative activity (RA) of Ago2 is measured according to eqn (1)–(3):

$$N_t = 206.2211 + 92.7939 \log_{10} C_t \quad (1)$$

$$N_i = 206.2211 + 92.7939 \log_{10} C_i \quad (2)$$

$$\mathrm{RA}\ (\%) = \frac{c_i}{c_t} \times 100\% = 10^{(N_i - N_t)/92.7939} \times 100\% \quad (3)$$

where N_t represents the Cy5 count in the presence of 50 nM Ago2 and N_i represents the Cy5 count in the presence of 50 nM Ago2 + inhibitor. C_t and C_i are calculated according to the linear correlation equation (Fig. 2C). The half maximal inhibitory concentration (IC_{50}, the concentration of the inhibitor that is required for 50% inhibition of Ago2 activity) is calculated to be 0.68 μM for ATA, 0.62 μM for SA, and 0.67 μM for 6-OHDA HCL, which are comparable to the reported IC_{50} values of ATA, suramin, and 6-OHDA HCL obtained by the fluorescence polarization assay.[41,42] We further applied this biosensor for Ago2

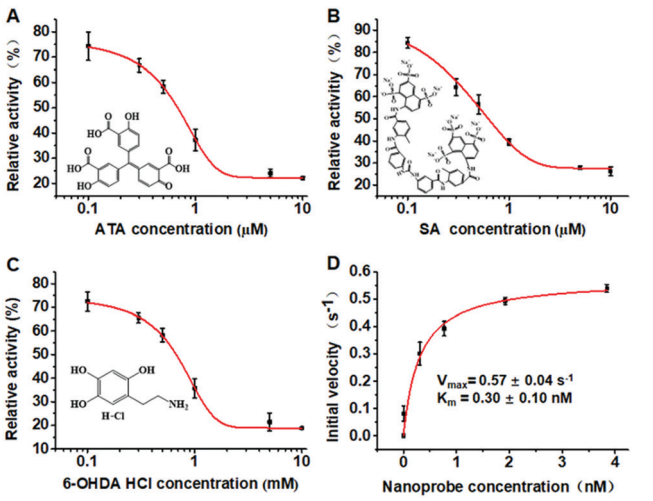

Fig. 4 (A–C) Variation of the relative activity of Ago2 with the concentrations of ATA (A), SA (B), and 6-OHDA HCL (C), respectively. (D) Variation of the initial velocity with the nanoprobe concentration. Error bars show the standard deviations of three experiments.

kinetic analysis (Fig. 4D). The initial velocity (V) in response to different concentrations of the AuNP nanoprobe is measured and fitted to the Michaelis–Menten equation:

$$V = \frac{V_{max}[S]}{K_m + [S]} \quad (4)$$

where [S] is the concentration of the nanoprobe, V_{max} is the maximum initial velocity, and K_m is the Michaelis–Menten constant.[43,44] The initial velocity enhances with the increasing concentration of the nanoprobe from 0 to 4 nM, and the V_{max} and K_m are determined to be 0.57 s^{-1} and 0.30 nM, respectively. These results indicated that the proposed nanosensor is suitable for Ago2 inhibitor screening and kinetic analysis.

3.6 Cellular Ago2 activity assay

We further measured the Cy5 signal in response to different numbers of cells including the human cervical carcinoma cell line (HeLa cells), human lung adenocarcinoma cell line (A549 cells), human breast cancer cell line (MCF-7 cells), and human colon cancer cell line (HCT116 cells). As shown in Fig. 5A, in contrast to the low signal obtained in the control without any cell extracts, high Cy5 counts are generated in HeLa cells, A549 cells, MCF-7 cells, and HCT116 cells, with the Cy5 signal decreasing in the order of HeLa cells > A549 cells > MCF-7 cells > HCT116 cells, consistent with previous research.[45,46] Moreover, the addition of Ago2 inhibitors (*i.e.*, ATA, SA, and 6-OHDA HCL) can induce the decrease of the Cy5 signal by 67.5%, 79.0% and 81.5%, respectively. In addition, the Cy5 count increases with the HeLa cell number from 0 to 10 000 cells (Fig. 5B), and a linear correlation is obtained between the Cy5 count (N) and cell number (X) from 5 to 1000 cells with a regression equation of $N = 127.19 \log_{10} X - 30.50$ ($R^2 = 0.9916$). These results demonstrate that the proposed biosensor can be applied for accurate and sensitive quantification of endogenous Ago2 activity in complex biological samples.

We further employed the proposed nanosensor to image the intracellular Ago2 activity in live HeLa cells. When the nanoprobe is absent (Fig. 6A), no fluorescence signal is observed.

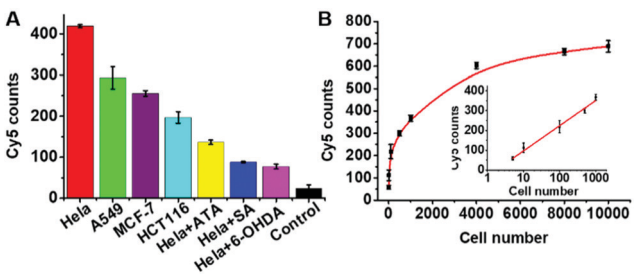

Fig. 5 (A) Measurement of the Cy5 count in response to cell extracts (equivalent to 10 000 cells) of HeLa cells (red column), A549 cells (green column), MCF-7 cells (purple column), HCT116 cells (cyan column), HeLa cells + 300 μM ATA (yellow column), HeLa cells + 50 μM SA (blue column), HeLa cells + 20 μM 6-OHDA HCL (pink column), and the control group without any cell extracts (black column). (B) Measurement of the Cy5 count in response to the HeLa cell number from 0 to 10 000 cells. Error bars represent the standard deviations of three experiments.

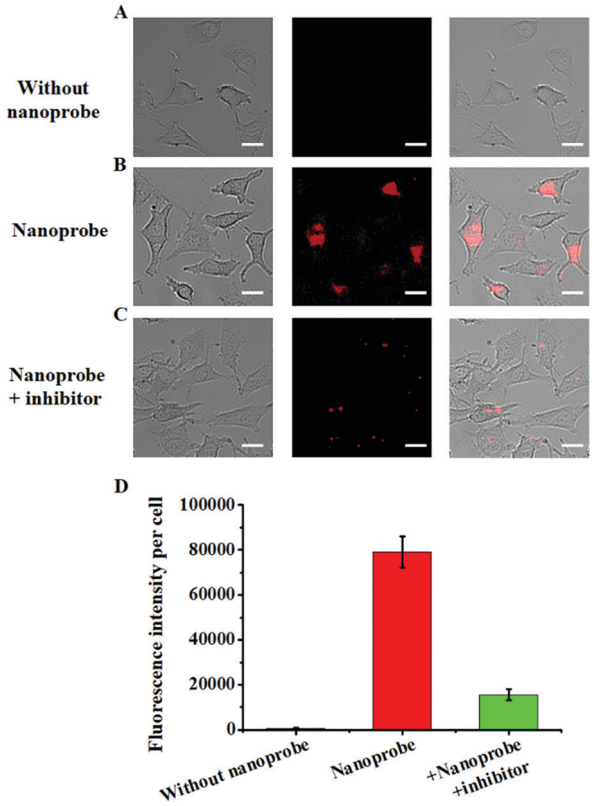

Fig. 6 (A-C) Imaging of Ago2 activity in HeLa cells under different conditions: (A) without the nanoprobe and with the (B) nanoprobe and (C) nanoprobe + inhibitor. The scale bar is 2 μm. (D) Fluorescence intensity per cell in response to the control group without the nanoprobe (black column) and with the nanoprobe (red column) and nanoprobe + inhibitor (green column). Error bars represent the standard deviations of three experiments.

In contrast, distinct fluorescence signals are observed in the presence of the nanosensor (Fig. 6B), suggesting the Ago2-induced cleavage of the nanoprobe and recovery of the fluorescence signal. After incubation of HeLa cells with the Ago2 inhibitor ATA, the Cy5 fluorescence signal decreases (Fig. 6B), indicating the efficient inhibition of intracellular Ago2 by ATA. We further quantified the fluorescence signal in live cell imaging. Negligible fluorescence is produced when the nanoprobe is absent (Fig. 6D, black column), and the signal produced by the nanoprobe + ATA group (Fig. 6D, green column) decreases by 80.35% compared with that produced by the nanoprobe only (Fig. 6D, red column). These results demonstrate that the proposed nanosensor can be applied for the imaging of intracellular Ago2 activity in live cells.

4 Conclusions

In summary, we have developed a new AuNP-based single-molecule biosensor for simple and sensitive detection of Ago2 activity. The self-assembly of multiple signal probes on a single AuNP facilitates the construction of a fluorescence-quenched and Ago2-responsive AuNP probe, enabling simple and sensitive

detection of Ago2 activity without the need for any extra antibodies and enzymes. The AuNP nanoprobe can greatly improve the Ago2 cleavage efficiency through increasing the local concentration of substrate signal probes. This single-molecule biosensor can sensitively detect Ago2 with a limit of detection of 9.12 pM, which is superior to the reported Ago2 assays.[19–22] Moreover, it can be successfully applied for the screening of inhibitors, analysis of kinetic parameters, and the imaging of intracellular Ago2 activity in live cells, holding great promise in Ago2-related fundamental research, drug discovery, and disease diagnosis.

Conflicts of interest

There are no conflicts to declare.

Acknowledgements

This work was supported by the National Natural Science Foundation of China (grant no. 21735003 and 22174017) and the Award for Team Leader Program of Taishan Scholars of Shandong Province, China.

Notes and references

1 A. Boland, F. Tritschler, S. Heimstädt, E. Izaurralde and O. Weichenrieder, *EMBO Rep.*, 2010, **11**, 522–527.
2 D. H. Kim, L. M. Villeneuve, K. V. Morris and J. J. Rossi, *Nat. Struct. Mol. Biol.*, 2006, **13**, 793.
3 G. Meister and T. Tuschl, *Nature*, 2004, **431**, 343.
4 G. Meister, *Nat. Rev. Genet.*, 2013, **14**, 447–459.
5 E. J. Sontheimer and R. W. Carthew, *Science*, 2004, **305**, 1409–1410.
6 L. L. Israel, E. Lellouche, R. S. Kenett, O. Green, S. Michaeli and J. P. Lellouche, *J. Mater. Chem. B*, 2014, **2**, 6215–6225.
7 G. Stefani and F. J. Slack, *Nat. Rev. Mol. Cell Biol.*, 2008, **9**, 219–230.
8 A. Mallory and H. Vaucheret, *Plant Cell*, 2010, **22**, 3879–3889.
9 T. M. Hall, *Structure*, 2005, **13**, 1403–1408.
10 D. O'Carroll, I. Mecklenbrauker, P. P. Das, A. Santana, U. Koenig, A. J. Enright, E. A. Miska and A. Tarakhovsky, *Genes Dev.*, 2007, **21**, 1999–2004.
11 J. Shen, W. Y. Xia, Y. B. Khotskaya, L. F. Huo, K. Nakanishi, S. O. Lim, Y. Du, Y. Wang, W. C. Chang, C. H. Chen, J. L. Hsu, Y. Wu, Y. C. Lam, B. P. James, X. P. Liu, C. G. Liu, D. J. Patel and M. C. Hung, *Nature*, 2013, **497**, 383–387.
12 J. R. Cubillos-Ruiz, J. R. Baird, A. J. Tesone, M. R. Rutkowski, U. K. Scarlett, A. L. Camposeco-Jacobs, J. Anadon-Arnillas, N. M. Harwood, M. Korc, S. N. Fiering, L. F. Sempere and J. R. Conejo-Garcia, *Cancer Res.*, 2012, **72**, 1683–1693.
13 O. Vaksman, T. E. Hetland, C. G. Trope, R. Reich and B. Davidson, *Hum. Pathol.*, 2012, **43**, 2062–2069.
14 J. Zhang, X. S. Fan, C. X. Wang, B. Liu, Q. Li and X. J. Zhou, *Med. Oncol.*, 2013, **30**, 628.
15 S. Diederichs, S. Jung, S. M. Rothenberg, G. A. Smolen, B. G. Mlody and D. A. Habert, *Proc. Natl. Acad. Sci. U. S. A.*, 2008, **105**, 9284–9289.
16 X. X. Zhang, P. R. Graves and Y. Zeng, *Biochim. Biophys. Acta, Gene Regul. Mech.*, 2009, **1789**, 153–159.
17 K. Okamura, A. Ishizuka, H. Siomi and M. C. Siomi, *Genes Dev.*, 2004, **18**, 1655–1666.
18 K. Ikeda, M. Satoh, K. M. Pauley, M. J. Fritzler, W. H. Reeves and E. K. L. Chan, *J. Immunol. Methods*, 2006, **317**, 38–44.
19 N. N. Yang, Y. Cao, P. Han, X. J. Zhu, L. Z. Sun and G. X. Li, *Anal. Chem.*, 2012, **84**, 2492–2497.
20 F. Li, P. Li, L. Yang and B. Tang, *Chem. Commun.*, 2012, **48**, 12192–12194.
21 K. Zhang, W. T. Huang, Y. Huang, H. Li, K. Wang, X. Zhu and M. H. Xie, *Anal. Chem.*, 2019, **91**, 7086–7096.
22 F. Li, M. Q. Chen, X. Z. Sun, X. Z. Wang and P. Li, *Sens. Actuators, B*, 2013, **182**, 156–160.
23 M. Hesse and C. Arenz, *ChemBioChem*, 2016, **17**, 304–307.
24 D. Zhang, F. Ma, J. Leng and C.-Y. Zhang, *Chem. Commun.*, 2018, **54**, 13678–13681.
25 Y. W. C. Cao, R. C. Jin and C. A. Mirkin, *Science*, 2002, **297**, 1536–1540.
26 Y. Hu, M. Xu, Y. Liu, X. Xie, W. Bao, A. Song and J. Hao, *J. Mater. Chem. B*, 2017, **5**, 1174–1181.
27 O. V. Pham-Nguyen, J. W. Lee, Y. Park, S. Jin, S. R. Kim, Y. M. Jung and H. S. Yoo, *J. Mater. Chem. B*, 2021, **9**, 9700–9710.
28 Q. Wu, K. Wang, X. Wang, G. Liang and J. Li, *J. Mater. Chem. B*, 2020, **8**, 3016–3027.
29 F. Ma, Q. Wang, Q. Xu and C.-Y. Zhang, *Anal. Chem.*, 2021, **93**, 15124–15132.
30 X. Yang, Y. Tang, S. D. Mason, J. Chen and F. Li, *ACS Nano*, 2016, **10**, 2324–2330.
31 F. V. Rivas, N. H. Tolia, J.-J. Song, J. P. Aragon, J. Liu, G. J. Hannon and L. Joshua-Tor, *Nat. Struct. Mol. Biol.*, 2005, **12**, 340–349.
32 F. Ma, Y. Li, B. Tang and C.-Y. Zhang, *Acc. Chem. Res.*, 2016, **49**, 1722–1730.
33 S. Jiang, P. Wang, C. C. Li, L. Cui, Y. Li and C. Y. Zhang, *J. Mater. Chem. B*, 2022, **10**, 3260–3267.
34 K. Q. Ye, L. Malinina and D. J. Patel, *Nature*, 2003, **426**, 874–878.
35 F. Ma, S. Jiang and C. Y. Zhang, *Biosens. Bioelectron.*, 2020, 157.
36 N. Yang, Y. Cao, P. Han, X. Zhu, L. Sun and G. Li, *Anal. Chem.*, 2012, **84**, 2492–2497.
37 K. Zhang, W. Huang, Y. Huang, H. Li, K. Wang, X. Zhu and M. Xie, *Anal. Chem.*, 2019, **91**, 7086–7096.
38 F. Ma, Y. Yang and C.-Y. Zhang, *Anal. Chem.*, 2014, **86**, 6006–6011.
39 W. Bode, D. Turk and A. Karshikov, *Protein Sci.*, 1992, **1**, 426–471.
40 D. D. Zhang, Y. R. Meng and C.-Y. Zhang, *Chem. Commun.*, 2020, **56**, 213–216.
41 G. S. Tan, C. H. Chiu, B. G. Garchow, D. Metzler, S. L. Diamond and M. Kiriakidou, *ACS Chem. Biol.*, 2012, **7**, 402–409.

42 Z. Wang, X. Wu, L. Liu, L. Xu, H. Kuang and C. Xu, *J. Mater. Chem. B*, 2019, **7**, 6383–6389.
43 G. Yang, Y. Lu, Y. Li, M. Ying, H. Pan, J. Qi and M. Du, *J. Mater. Chem. B*, 2021, **9**, 4663–4669.
44 X. Wu, T. Chen, J. Wang and G. Yang, *J. Mater. Chem. B*, 2018, **6**, 105–111.
45 L. G. Wu, J. H. Fan and J. G. Belasco, *Curr. Biol.*, 2008, **18**, 1327–1332.
46 E. Prodromaki, A. Korpetinou, E. Giannopoulou, E. Vlotinou, M. Chatziathanasiadou, N. I. Papachristou, C. D. Scopa, H. Papadaki, H. P. Kalofonos and D. J. Papachristou, *Cell. Oncol.*, 2015, **38**, 307–317.